Experimental Thermal and Fluid Science 62 (2015) 109–121

Contents lists available at ScienceDirect

Experimental Thermal and Fluid Science

journal homepage: www.elsevier.com/locate/etfs

Experimental studies on the shape and motion of air bubbles in viscous liquids

Liu Liu, Hongjie Yan *, Guojian Zhao

School of Energy Science and Engineering, Central South University, 410083 Changsha, China

ARTICLE INFO

Article history:
Received 13 June 2014
Received in revised form 14 November 2014
Accepted 15 November 2014
Available online 24 December 2014

Keywords:
Bubble dynamic characteristics
Bubble shape
Bubble trajectory
Bubble velocity
Gas–liquid two-phase flow

ABSTRACT

This paper is concerned with single bubble dynamics over a wide experimental data set in stagnant water and glycerol aqueous solution. The bubble trajectory in three-dimensional space was deduced by analyzing the bubble characteristics in two-dimensional plane captured by a single high-speed camera and the bubble trajectory in the water was ascertained by this method. Bubble shape, trajectory and terminal velocity in water, which closely related and strongly influenced by each other, are not only determined by bubble diameter, but also dramatically influenced by nozzle diameters, i.e. the bubble dynamics is sensitive to the disturbance of detachment process. The bubbles remain spherical and rise up rectilinearly when their diameters are small enough. Otherwise, the bubbles begin to deform to ellipsoidal, oblate ellipsoidal, or cap shape, with surface wobbling strongly, and proceed in a zigzagging, helical, nearly zigzagging or helical motion. In this case, periodic oscillations occur at the velocity and aspect ratio of the bubbles. Moreover, there exists an inverse function relationship between them, a large deformation, i.e. a small aspect ratio will lead to a high velocity and vice versa. However, in glycerol aqueous solution, bubble shape, trajectory and velocity is stable under a certain bubble diameter. In the water, bubble shape is mainly dominated by the inertial force and surface tension, and the influence caused by the viscous force could be neglected. The influence of gravity should be taken into consideration if the bubble diameter is large enough. However, the bubble shape is mainly dominated by the viscous force, surface tension and inertial force in the glycerol aqueous solution. Available correlations in the literature do not give fully satisfactory results in predicting aspect ratio, and new correlations combined Weber number with Eötvös number and Weber number with Reynolds number were proposed to correlate bubble shape in water and glycerol aqueous solution, respectively, showing that a good relevance between them in the range of the present experimental data set.

1. Introduction

A lot of work had been performed to study the single bubbles rising behavior in stagnant liquids, which revealed the key parameters that affect the gas–liquid two-phase flow are bubble size, shape, trajectory, and velocity [1–3]. It has guiding significance for in-depth study of bubble dynamics in gas–liquid two-phase flow to solve many engineering problems. Researches on the bubble dynamics have been conducted for decades, and many achievements have been accomplished by using theoretical analysis [4–8], experimental measurement [9–14] and numerical simulation [15–20], showing that the interactions between gas and liquid, i.e. viscous force, gravity, surface tension, and inertial force, mainly dominate the behavior of bubble dynamics.

The bubble shape, which is a quite important parameter of the bubble dynamics, is mainly related to the physical properties of fluid, bubble size, bubble velocity, etc. Since the regime map of the bubble shape, aimed at describing the relationship between bubble shape and dimensionless parameters Eötvös number ($Eo = gd^2(\rho_l - \rho_g)/\sigma$), Reynolds number ($Re = \rho_l V_T d/\mu_l$) and Morton number $\left(Mo = (\rho_l - \rho_g)g\mu_l^4/\sigma^3\rho_l^2\right)$ has been proposed by Grace [1], various researchers [1,3,17,18,21,22] have carried out plenty of studies on the bubble shape in different fluids and their results mostly coincide with the regime map of the bubble shape. Almost all the studies adopted aspect ratio, E, defined as the ratio of minor to major axis of the bubble, i.e. the ratio of height to width, to describe the bubble shape, and successfully obtained a series of empirical correlations by correlating aspect ratio to Eötvös number [23,24], Weber number $\left(We = \rho_l V_T^2 d/\sigma\right)$ [23,25–28] and Tadaki number ($Ta = ReMo^{0.23}$) [29–31], which indicates that it is reasonable to correlate aspect ratio as a function of different

* Corresponding author. Tel./fax: +86 0731 88830239.
E-mail addresses: znliuliu@163.com (L. Liu), s-rfy@csu.edu.cn (H. Yan), csu_zgj@163.com (G. Zhao).

http://dx.doi.org/10.1016/j.expthermflusci.2014.11.018
0894-1777/

Nomenclature

a	undetermined coefficients (–)
b	undetermined coefficients (–)
c	undetermined coefficients (–)
d	bubbles diameter (mm)
Do	inner diameter of nozzle (mm)
e	undetermined coefficients (–)
E	aspect ratio (–)
Eo	Eötvös number (–)
g	gravitational acceleration (m/s^2)
h	bubble height (mm)
IL	dimensionless number (–)
Mo	Morton number (–)
n	number of data points (–)
r	correlation coefficient (–)
Re	Reynolds number (–)
SSE	residual sum of squares (–)
StD	standard deviation (–)
T	Temperature (°C)
Ta	Tadaki number (–)
V	bubble velocity (m/s)
V_h	bubble horizontal velocity (m/s)
V_T	bubble terminal velocity (m/s)
V_v	bubble vertical velocity (m/s)
w	bubble width (mm)
We	Weber number (–)
t	time (s)
x	bubble horizontal position (mm)
z	distance above the nozzle surface (m/s)

Greek symbols

μ	dynamic viscosity (kg/s^2 m)
ρ	density (kg/m^3)
σ	surface tension (N/m)

Subscripts

g	pertains to the gas phase
h	pertains to the horizontal position
l	pertains to the liquid phase
v	pertains to the vertical position

dimensionless parameters. Meanwhile, bubbles rising in liquids performed rectilinear, zigzag or helical motions [32–35]. Saffman [36] studied the motion of air bubbles in water and pointed out that bubbles always keeps rectilinearly up with its diameter less than 1.4 mm, otherwise, it is sensitive to disturbance and the trajectory changes from linear to zigzag or helical. Benjamin [37] studied the ratio of the helical radius of the bubble motion to the bubble equivalent radius. Similarly, de Vries et al. [33] also got this parameter by experimental study, but the result was almost 23 times greater than Benjamin's. Brücker [38] investigated the bubble shape oscillation and trajectory transition process, which indicates that, the bubble rises rectilinearly in the initial rising process. After the bubble rises more than 25 mm, the oscillating of bubble surface is strong and the bubble trajectory changes from linear to helical. Ellingsen and Risso [39] studied the bubble motion characteristics in quiescent water. Tomiyama et al. [11] investigated the bubble trajectories and the rising process in different fluid, and the results showed that the bubble formation process has significant influence on the trajectory, deformation and velocity. The above research work revealed that the bubble formation process may be the reason leading to different rising trajectories. Also, for the same size of bubbles, they show different trajectories during the rising process, suggesting that the bubble rising process is influenced by different factors, which are far from fully understood. Therefore, further work should be carried out to reveal the mechanics. In addition, the rising velocity is also one of the fundamental parameters in gas–liquid two-phase flow. Although a lot of research work [11,31,40–43] has been made on the prediction of bubble terminal velocity, it is very difficult to predict the bubble terminal velocity accurately, due to the fact that the bubble rising terminal velocity is related to many factors such as fluid physical properties, liquid pollution degree, bubble size, bubble shape, bubble trajectory and injection mode. The study of Clift et al. [2] showed that, the contaminant in the liquid affect the interface between the bubble and liquid, which has a great impact on the bubble terminal velocity. Rodrigue et al. [44] also studied the influence of the surfactant on the bubble terminal velocity and pointed out that the surfactant could promote the formation of bubble rigid surface, leading to the drag increasing and due to the result that the bubble rising terminal velocity less than that of the same diameter in water. Aybers and Tapucu [45,46] measured the bubble instantaneous velocity in water, showing that after the bubble detached the nozzle for a certain distance, the bubble velocity reached the maximum value, and then decreased slowly, finally reached stable. The research by Tomiyama et al. [11] showed that the bubble terminal velocity is closely related to the ways of bubble injection, which are divided into "controlled injection" and "direct injection". Celata et al. [47,48] studied bubble rising velocity under different injection modes in pure water, polluted water and pure FC-72 liquid. The result indicated that the purity of liquid has a great effect on the bubble terminal rising velocity and the bubble shape. The bubble aspect ratio interacts with the bubble terminal velocity each other. Okawa et al. [24] researched the motion characterization of spherical and ellipsoidal bubble diameter within 0.6–3.7 mm in room and high temperature water, and confirmed that the bubble velocity is affected by the way of injection in room temperature water. In high temperature water, the way of injection also affects the bubble velocity, but the effect of the initial deformation under different ways of injection to the bubble velocity decreases compared in room temperature water. Rodrigue et al. [44] showed that the bubble terminal velocity and the diameter are in the linear relationship under different concentration glycerin water liquid. At the same time, because of the liquid viscous force, the bubble terminal rising velocity decreases with the viscosity increasing.

In this study, a single bubble dynamics was investigated experimentally in water and glycerin water solution using the high-speed photography instrument combined with digital image processing algorithm. The aim of this paper is to discuss the bubble dynamic behavior in different liquid phase, including water and glycerol aqueous solution, to confirm the influence of *Mo*, *Eo*, *Re*, *We* and other dimensionless numbers on the bubble characteristics. It mainly focuses influence of buoyancy, inertial force, surface tension, viscosity, nozzle diameter, and physical properties of the continuous phase on the bubble shape, trajectory and velocity.

2. Experiment

2.1. Experimental apparatus and procedure

The experimental apparatus is shown schematically in Fig. 1.

The experiments were carried out in a rectangular organic glass tank filled with different liquids, water or glycerin aqueous solution. The width, depth and height of the tank were 150, 150 and 500 mm, respectively. The stainless steel nozzle with a flat opening was installed at the center of the bottom of the tank. The distance

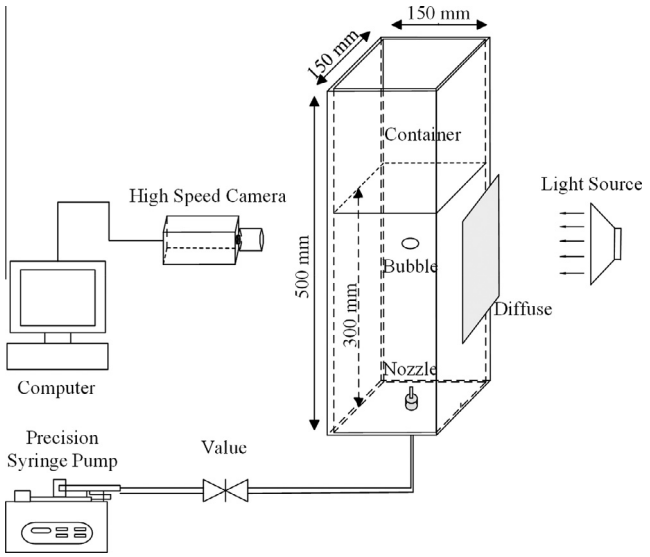

Fig. 1. Sketch of the experimental apparatus.

between the upper surface of nozzle and the bottom of tank was 30 mm. Water or glycerin aqueous solution that had been sufficiently exposed to ambient temperature was put into the tank as liquid phase. The liquid phase was kept 300 mm above the nozzle. With the help of a precision syringe pump, air was produced and transported into the nozzle through the pipeline, and then a single bubble was generated at the nozzle by controlling the flow of the syringe pump. In order to minimize the influence of the subsequent bubble, the time interval between the adjacent two bubbles should be sufficiently long.

The bubble behavior was recorded by a high-speed camera (Motion Pro X3, REDLAKE Co., USA). The frame rate of the camera could be up to 3273 fps. The image with a resolution of $1280 * 1024$ pixels was produced by an Avenir lens, whose focal length ranged from 16 to 160 mm. The illumination of the test region was provided by a LED lamp behind the rectangular tank, installed with a parchment paper as a light diffuse. The image sequences obtained were then analyzed by a digital image processing algorithm based on Matlab software, which is specifically developed in order to calculate the bubble characteristics.

The densities of liquid phase were measured by a hydrometer and the liquid viscosities were by a rotary viscometer (DV-II, BROOKFIELD Co., USA). The surface tensions of liquid were measured by a surface tension meter (BZY-B, SHANGHAI FANGRUI INSTRUMENT Co., China). The physical properties of the liquid are summarized in Table 1, in which S1 to S4 represent various glycerin aqueous solutions with different viscosities.

2.2. Measurement methods

Fig. 2 shows schematic diagrams of typical bubble shapes projected on the plane perpendicular to the photographing direction of the camera.

The bubble equivalent diameter d is evaluated as the same volume by considering bubbles as an ideal symmetrical body of revolution along the minor axis, without considering the bubble wobbling and non-axisymmetric characteristics. The evaluation of the aspect ratio is also under this assumption and then defined by Eq. (1).

$$E = h/w \tag{1}$$

In the water, the equivalent diameter and aspect ratio of bubbles are easy to calculate in the case that bubble shape remains spherical or ellipsoidal when the diameter is sufficiently small. However, the bubble shape deforms to oblate ellipsoidal, then to spherical-cap or ellipsoidal-cap with the surface wobbling along the observed path when increasing the bubble diameter [2]. In these cases, the equivalent diameter and aspect ratio are quite difficult to be evaluated accurately only from one direction by a camera for bubbles with shape and/or motion oscillation, especially for those bubbles with zigzag or helical motion whose equivalent diameter and aspect ratio might depend on relative angle between the motion plane and the observation plane. In order to evaluate the reliability of the data obtained only from one direction by a single camera, a series of experiments have been performed by recording the bubble images through two perpendicular directions with two cameras A and B. The two measured diameter and aspect ratio of bubbles are plotted in Figs. 3 and 4, respectively. As indicated from Figs. 3 and 4, most data agree with each other within the error of 10%. Hence, we may have the conclusion that the data obtained by a single camera from one direction is expected to be reasonably right.

2.3. Experimental uncertainties

The uncertainty of bubble equivalent diameter has two main sources. The first source is due to the error in detecting the bubble edge in the digital image processing. The second is the calculation of the equivalent diameter by assuming that the bubble is a symmetrical body of revolution. After much trial and error, it is indicated that the maximum error in determining the bubble edge is ±1 pixel. Hence, when the bubble diameter is less than 0.5 mm, at this time, the minimum diameter of the captured bubble is 0.12 mm and the spatial resolution is 0.01 mm/pixel, so the maximum error is ±8.33% and the minimum error is ±2%. When the bubble diameter range from 0.5 to 1 mm, the maximum error is ±4% and the minimum error is ±2%. When the bubble diameter is between 1 and 2.5 mm, the maximum error is ±4% and the minimum error is ±1.6%; when the bubble diameter is larger than 2.5 mm, the maximum diameter of the captured bubble is 22.04 mm, so the maximum error is ±4% and the minimum error is ±0.45%. For the second error, the maximum is less than 5% by the analysis.

According to the studies by Celata et al. [46,47], the uncertainty of the bubble shape can be evaluated by considering for each bubble the root mean square of the aspect ratio along the observed path of the bubble. Therefore, bubble oscillations and non-axisymmetric characteristics due to the zigzagging, helical

Table 1
Physical properties of the liquid phase.

Liquid phase		Density/kg m^{-3}	Viscosity/mPa s	Surface tension/mN m^{-1}	*Mo*
Water (T = 8 °C)		999.8	1.38	74	8.73E−11
Water (T = 29 °C)		996.7	0.86	72	1.48E−11
Glycerin aqueous solution (T = 8 °C)	S1	1246.1	622.2	65	4.29
	S2	1236.0	306.1	65	0.253
	S3	1220.3	115.3	66	0.004887
	S4	1206.5	63.0	67	0.0004256

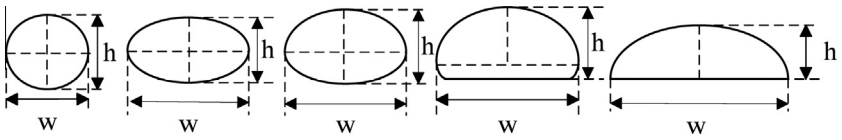

Fig. 2. Schematic diagrams of typical bubble shapes.

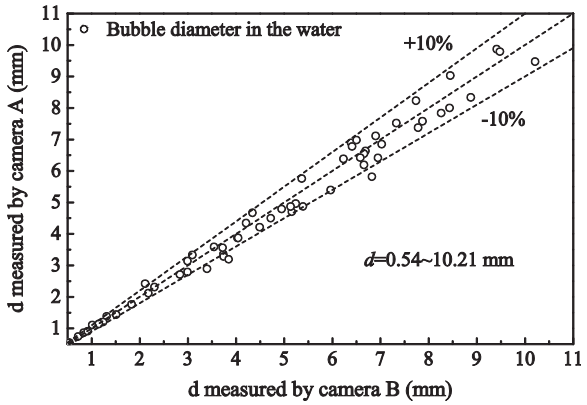

Fig. 3. Bubble diameter measured by two cameras.

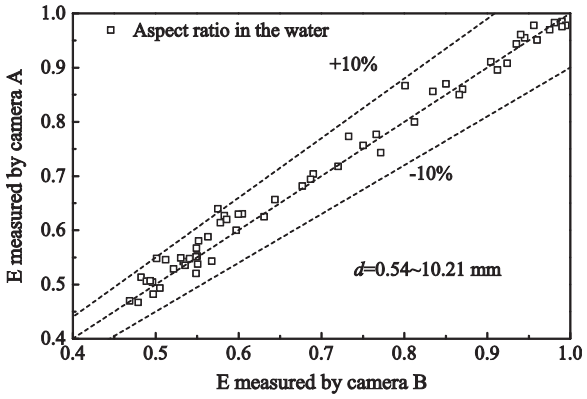

Fig. 4. Bubble aspect ratio measured by two cameras.

motion or surface wobbling, as well as the error in detecting the bubble edge are all taken into account by this method. The average root mean square is ±5.57% (from ±0.31% to ±16.42%) in the water and 0.94% (from ±0.20% to ±2.96%) in glycerin aqueous solution.

The uncertainty of the ensemble averaged terminal velocity also can be evaluated by considering for each bubble the root mean square of the velocity along the observed path of the bubble where bubble has reached a stable state after rising a certain distance. The average root mean square is ±1.20% (from ±0.04% to ±4.65%) in the water by analyzing the velocity data.

3. Results and discussion

3.1. Bubble ascent behavior in water

3.1.1. Bubble rising process after detaching from the nozzle

After the bubble detaches from the nozzle, the buoyant force makes it ascent in the liquid phase. Fig. 5 shows image sequence of bubble motion with different diameter generated under various nozzles. The bubble images in the same figure are the same bubble and the time internal between two consecutive images is 0.008 s. As shown in Fig. 5(a), after the bubble of a small size detaches from the nozzle, its trajectory shows a rectilinear behavior and the shape retains spherical along the path. With the increase of bubble diameter, the bubbles exhibit rectilinear path firstly. After bubbles rise for a certain distance, the path begins to deviate from the straight line, then transform to a zigzag motion and finally retain zigzag rising behavior. Meanwhile, the bubbles shape also turns from spherical to ellipsoidal or oblate ellipsoidal, as shown in Fig. 5(c)–(e). However, with the bubble diameter increasing continually, as shown in Fig. 5(f), the bubbles shape changes to oblate flat, with surface oscillating strongly, and the path shows neither severe rectilinear nor zigzagging, but presents nearly a zigzagging rising behavior. From the analysis above, the bubble trajectory keeps rectilinear for a certain distance and may continue to maintain or switch to a zigzagging or nearly zigzagging rising, which has been pointed out in many previous researches (e.g. [36,38,39]).

Bubble vertical velocity V_v, horizontal velocity V_h, and aspect ratio E as a function of the distance away from the nozzle surface z of two typical rising paths, i.e. rectilinear path (Fig. 5(b)) and zigzagging (Fig. 5(e)) path, are shown in Fig. 6. After detachment from the nozzle, the vertical velocity of bubble begins to rise rapidly while the aspect ratio decreases rapidly, as shown in Fig. 6(a). At the point of $z \approx 20$ mm, the vertical velocity reaches near 0.30 m/s and aspect ratio reduces to near 0.43, and then they all keeps constant along the path. Meanwhile, bubble horizontal velocity retains zero along the path where z less than 60 mm, and then decreases to the negative at the point $z \approx 60$ mm, which indicates that the bubble deviates from the straight direction and moves to left. After that, the horizontal velocity slowly decreased with the distance increasing. However, the bubble that follows a zigzagging rising path, as shown in Fig. 6(b), shows a different behavior between V_v, V_h, E and z. In this case, the bubble vertical velocity begins to rise rapidly, and horizontal velocity retains zero, while aspect ratio decreases rapidly immediately after bubble detaching from the nozzle. At the point of $z \approx 13$ mm, the bubble vertical velocity reaches the maximum value and the horizontal velocity maintains around zero, while the aspect ratio reaches the minimum value. Then the vertical velocity decreases, while the aspect ratio increases rapidly, and the horizontal velocity increases to a positive value. At the point of $z \approx 20$ mm, the vertical velocity reduces to the minimum value, while the aspect ratio E and the horizontal velocity reach the maximum value. For $z > 20$ mm, the vertical velocity begins to rise once again, while the aspect ratio and horizontal velocity begin to decrease, and finally they all repeat a behavior of period oscillation. As a result, we can draw a conclusion that the vertical velocity, horizontal velocity and the aspect ratio E of bubbles that show a rectilinear rising path would maintain a relatively stable state, in which the oscillation amplitude is very small. While bubbles that follow a zigzagging rising path would appear periodic oscillation in the vertical velocity, horizontal velocity and the aspect ratio E. Bubble trajectory, velocity and aspect ratio, are closely related and strongly influenced by each other.

3.1.2. Bubble rising process during the steady state

From the analysis above, it is obvious that the bubble velocity increases continually for certain distance after detaching from the nozzle and finally achieve nearly a steady state. By analyzing the bubble path and velocity under different conditions, we found

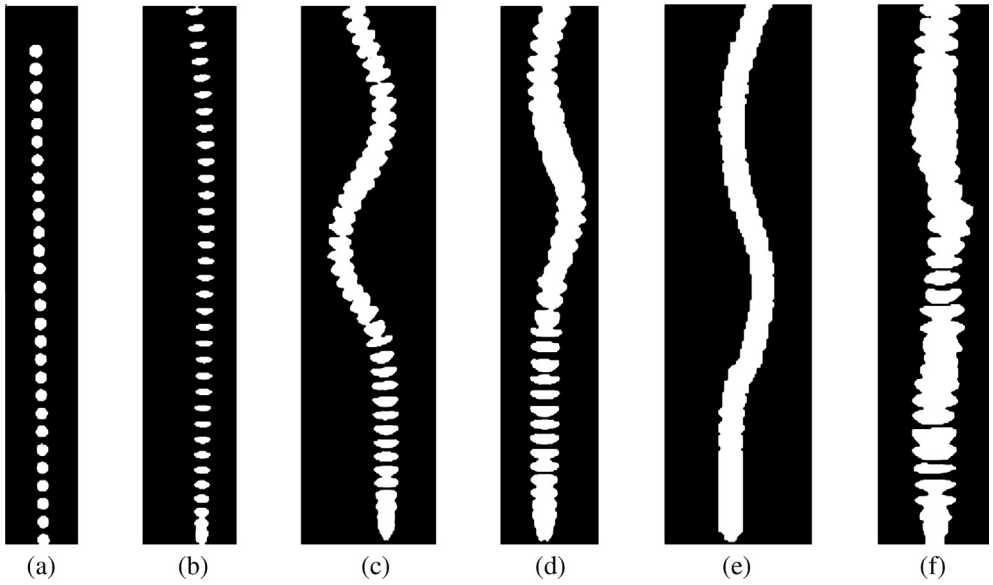

Fig. 5. Image motion sequence of different diameter bubbles generated under different nozzle diameters (a) Do = 7.7 mm, d = 0.87 mm; (b) Do = 0.6 mm, d = 2.01 mm; (c) Do = 1.2 mm, d = 2.80 mm; (d) Do = 1.6 mm, d = 3.01 mm; (e) Do = 2.0 mm, d = 2.77 mm; (f) Do = 4.0 mm, d = 5.31 mm.

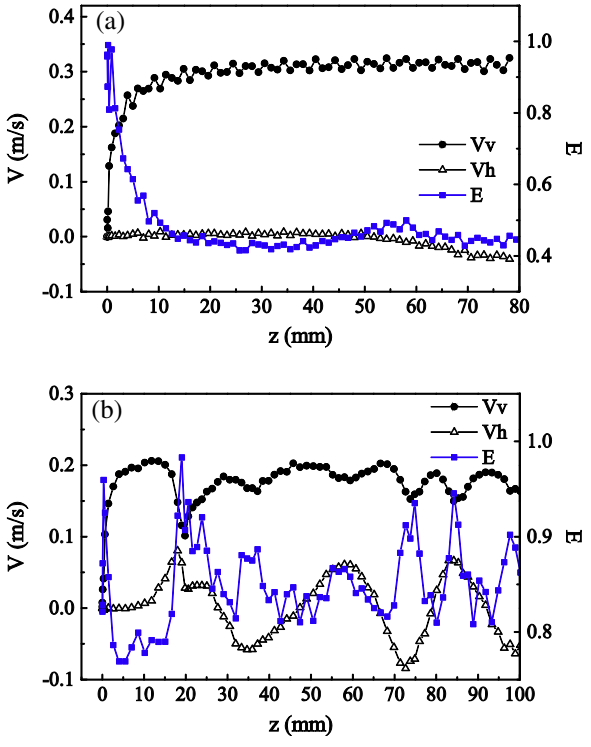

Fig. 6. Bubble vertical velocity V_v, horizontal velocity V_h, and aspect ratio E as a function of the distance above the nozzle surface (a) Do = 0.6 mm, d = 2.01 mm; (b) Do = 2.0 mm, d = 2.77 mm.

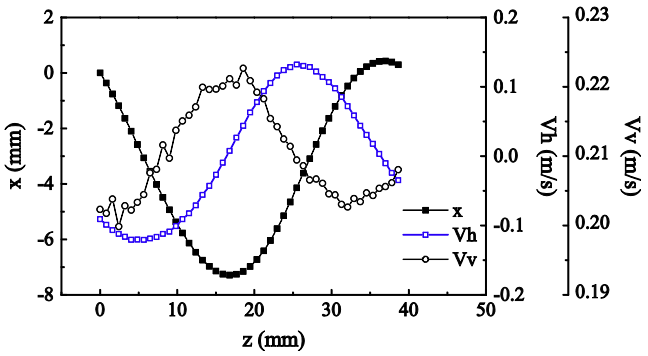

Fig. 7. Bubble horizontal position x, horizontal velocity V_h and vertical velocity V_v as a function of the distance above the nozzle surface z, d = 2.3 mm.

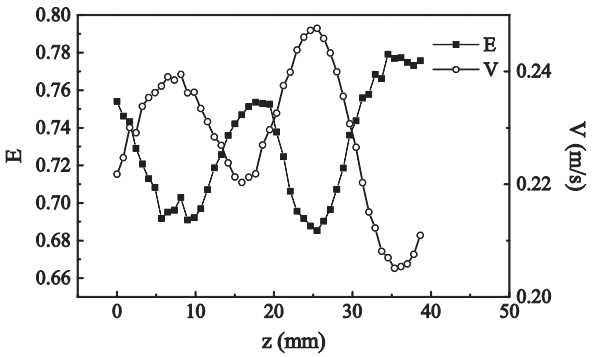

Fig. 8. Trend of aspect ratio and instantaneous velocity vs. distance above the nozzle surface.

that bubbles could reach a stable state after rising a distance of 150 mm. So the bubble image sequence in the range of 150–200 mm above the nozzle surface is chosen to analysis the rising behavior in the steady state.

As can be known from the Section 3.1.1, when bubbles rise rectilinearly, the velocity and aspect ratio would remain stable along the path. Nevertheless, when bubbles follow zigzag or helical rising, the trend of velocity and aspect ratio are different from those of the rectilinear trajectory. Figs. 7 and 8 show the trend of instantaneous velocity and aspect ratio vs. z for a typical zigzagging motion bubble. As shown in Figs. 7 and 8, when x is at the point of peak or trough in S shaped curve, the V_v and the E reach their maximum value, and the V_h retains 0, while the instantaneous velocity V reaches its minimum value. When x is at the center of the peak and trough in S shaped curve, the V_h achieves its maximum or minimum value, the V_v is between the peak and

trough, and the E reaches the minimum value, while the V reaches the maximum value. Furthermore, Fig. 8 shows that the bubble velocity V is an inverse function of the aspect ratio E, i.e. a bigger aspect ratio will result in a smaller velocity and vice versa. Therefore, it can be concluded that the bubble velocity is closely related to the bubble shape, a large deformation will lead to a high velocity and vice versa, which are in good agreement with the previous researches (e.g. [11,47,48]).

The literature [9,32–35,47] reported a lot of research about the bubble trajectory, which mostly concentrated on the spherical or ellipsoidal bubble with small diameters and usually studied three-dimensional trajectory of the bubble by photographing the bubble image sequence with two or more cameras. In present study, we try to deduce the trajectory of spherical, ellipsoidal, oblate, and cap shaped bubbles in three-dimensional space by analyzing the bubble characteristics in images captured by a single camera.

(a) Bubble trajectory is rectilinear

In the case of a rectilinear trajectory, the horizontal position x does not appear periodic oscillation, showing a linear relationship with vertical potion z, therefore the horizontal velocity V_h remains zero or constant, while the vertical velocity V_v keeps a constant value. Fig. 9 shows bubble vertical velocity V_v, horizontal velocity V_h, and horizontal position x as a function of the distance above the nozzle surface z, which indicates that the above deductions have a good agreement with experiments.

(b) Bubble trajectory is zigzag

In this case, if the photographing direction of the camera just parallels to the 2D plane of the bubble motion, the x shows a linear relationship with z, and the V_h remains 0, while V_v shows a periodic oscillation. Otherwise, all of the x, V_h and V_v show a periodic oscillation, and the oscillation frequency of V_v is double than x and V_h. In addition, when the x is at the point of crests or troughs of S shaped curve, the V_h changes to be 0, and the V_v reaches its maximum value. Besides, when the x is nearly at the midpoint between crests and troughs of S shaped curve, the V_h reaches its maximum or minimum value, while the V_v is nearly at center of peak and trough. Fig. 10 shows an example of zigzag paths observed in this work.

(c) Bubble trajectory is helical

In the case of a helical motion, the trajectory has no difference with the zigzag motion in the 2D plane of the bubble motion, i.e. they both show an S shaped curve. Therefore, it fails to deduce whether the bubble trajectory is zigzag or helical only by analyzing the bubble trajectory in the 2D image. However, as illustrated by Celata et al. [47], when the bubble shows a helical rising, the V_v remains stable and does not appear a regular periodic oscillation, which is essentially different from that in zigzag rising. Hence, the helical motion will be distinguished from the zigzag motion by comparing the characteristics of the V_v when both the bubble trajectory shows an S shaped curve and the V_h shows a periodic oscillation. Fig. 11 shows a typical example of a helical trajectory.

Bubble terminal velocity and aspect ratio vs. bubble diameter are respectively plotted in Figs. 12 and 13, along with the measurement error of all bubble data and the types of trajectory of each bubble are also illustrated by using the method introduced above.

It can be seen from Figs. 12 and 13 that bubble terminal velocity increases while aspect ratio decreases almost linearly with bubble diameter in the viscous force dominant regime where $d < 0.83$ mm and bubble trajectory all keeps rectilinear. Then, both terminal velocity and aspect ratio begin to widely scatter while bubble trajectory is likely to remain rectilinear or switch to be zigzag or helical with d increasing in the surface tension force dominant regime where $0.83 < d < 6$ mm. As a whole, the terminal velocity seems to be higher while aspect ratio to be lower for bubbles with helical trajectories than those bubbles with zigzag trajectories in this regime, which indicates that a bubble with low aspect ratio is more likely to result in a high terminal velocity and a helical rising path. Finally, the level of scatter tends to be quite weak and terminal velocity increases while aspect ratio decrease gradually in the inertial force dominant regime where $d > 6$ mm, and the bubble motion in this regime could be either zigzag or helical, without rectilinear motions occurring. In addition, in Figs. 12 and 13, it is noticeable that the terminal velocity can reach the peak value about 0.3 m/s and bubbles are likely to be spherical or ellipsoidal with a wide range of aspect ratio and a rectilinear, zigzag or helical rising path in the regime $1 < d < 2$ mm, especially at the regime $d \approx 1.5$ mm, showing that tremendous changes in bubble dynamics might occur in this regime. The results are well consistent compared with the studies by Tomiyama et al. [11], Okawa et al. [24] and Celata et al. [47].

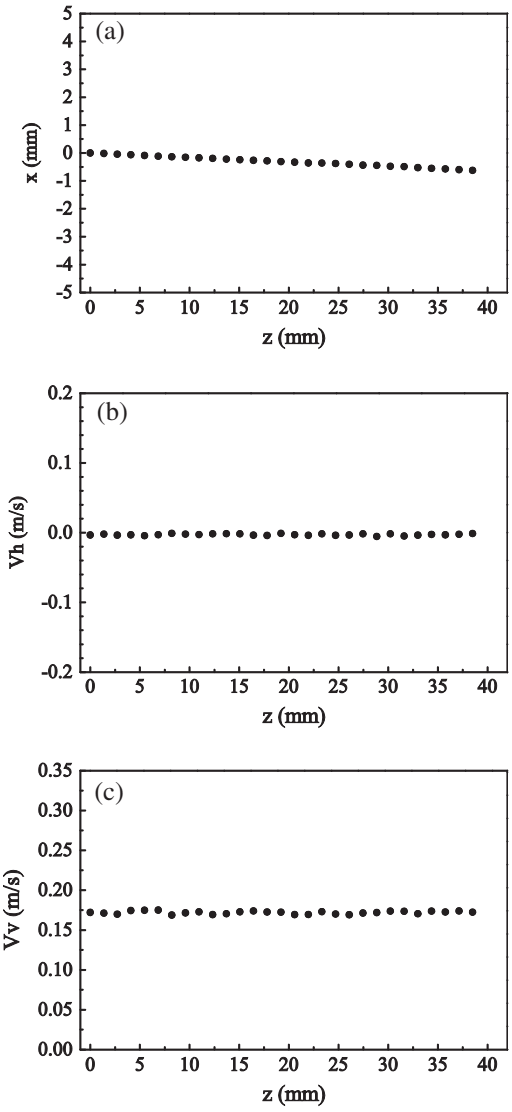

Fig. 9. Bubble horizontal position x, horizontal velocity V_h and vertical velocity V_v as a function of the distance above the nozzle surface z, $d = 0.87$ mm (a) horizontal position; (b) horizontal velocity; (c) vertical velocity.

3.2. Bubble ascent behavior in glycerin aqueous solution

Fig. 14(a)–(d) shows the image sequence of bubble motion with different diameter in glycerin aqueous solution S4. The time interval of two consecutive images is 0.036 s. As shown in figure, the trajectories of all bubbles are rectilinear. The shape of bubble with a small diameter is spherical as shown in Fig. 14(a). With the

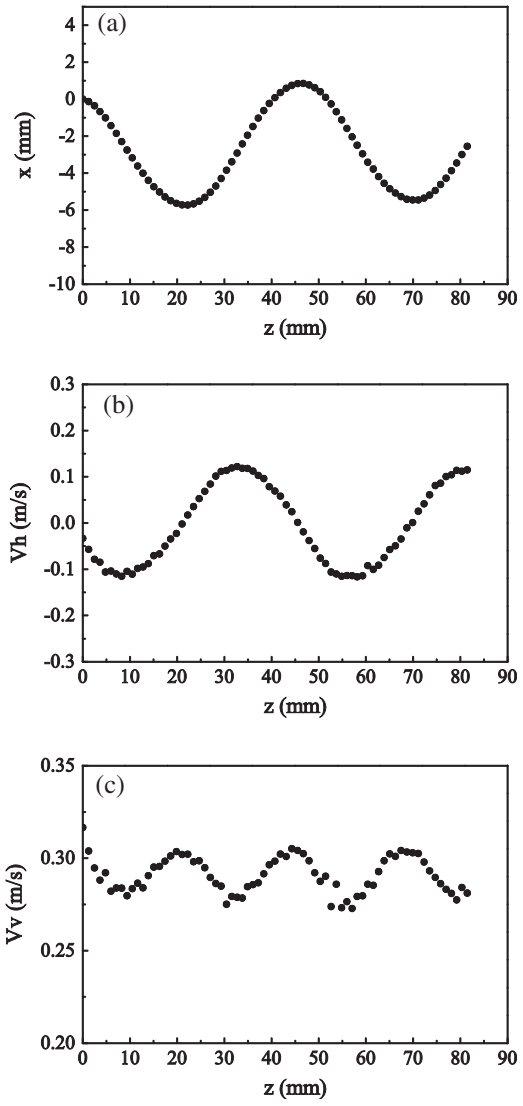

Fig. 10. Bubble horizontal position x, horizontal velocity V_h and vertical velocity V_v as a function of the distance above the nozzle surface z, d = 2.01 mm (a) horizontal position; (b) horizontal velocity; (c) vertical velocity.

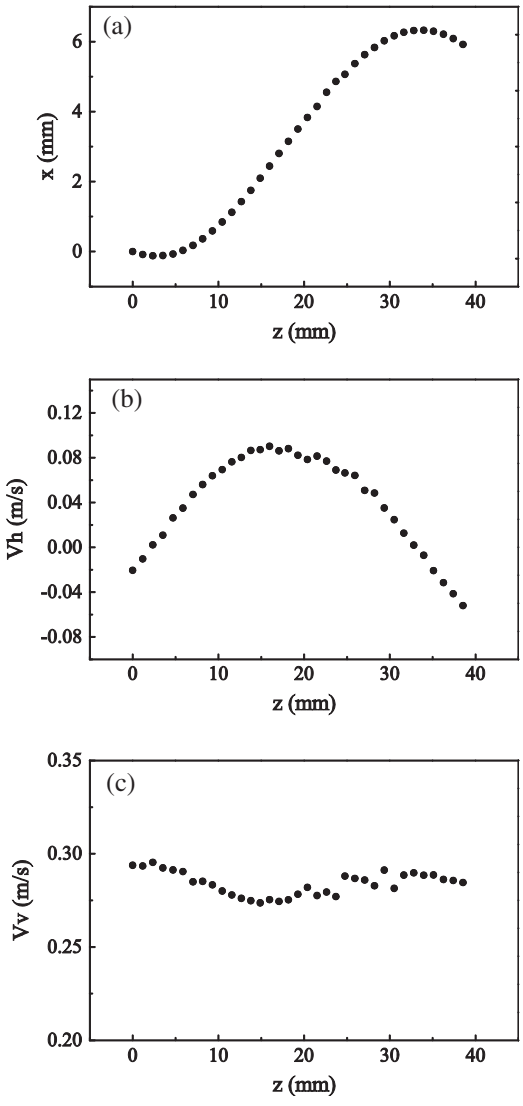

Fig. 11. Bubble horizontal position x, horizontal velocity V_h and vertical velocity V_v as a function of the distance above the nozzle surface z, d = 1.83 mm (a) horizontal position; (b) horizontal velocity; (c) vertical velocity.

increase of the bubble diameter, the bubbles deform from spheres to ellipsoid, and then to spherical cap shape, which are shown in Fig. 14(b)–(d).

The profiles of the instantaneous velocities of these bubbles during the formation and rising processes are shown in Fig. 15. As can be seen from figure, the instantaneous velocities increase slowly in bubble formation process, after the bubbles detach from the nozzle, due to the inertial and buoyancy force, the instantaneous velocities increase quickly, then, approach the terminal velocities and remain constant. As to the bubbles of d = 4.76 mm, d = 5.61 mm and d = 7.33 mm, the instantaneous velocities of them had a maximum value before approach the terminal state, then the instantaneous velocities decrease a little and finally tends to be stable. However, as to the bubble of d = 2.26 mm, the instantaneous velocity has kept increasing constantly, and finally achieved stability without experiencing a maximum value.

Figs. 16 and 17 show consecutive bubble images at different time of the bubble of d = 7.33 mm and 2.26 mm, respectively. As shown in Figs. 16 and 17, the peak velocity may be caused by the displacement of the center of gravity of the projection of the bubble. In Fig. 12, the bubble is about to detach from the nozzle at the point of t = 0 s, only the base of it keeping connected with

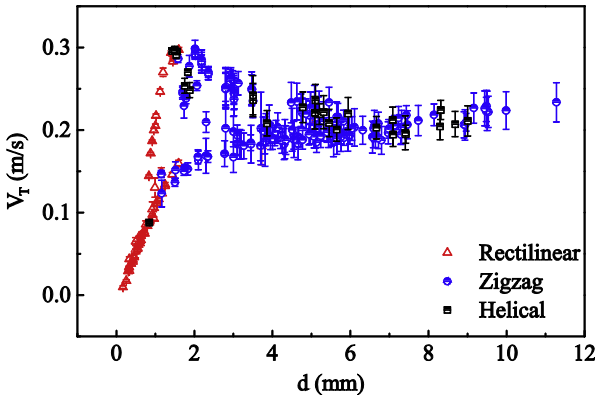

Fig. 12. Bubble terminal velocity V_T vs. bubble diameter d in water.

the nozzle. Then, after 0.004 s, the bubble detaches from the nozzle and the bubble necking begins to shrink immediately. At the point of t = 0.008 s, due to the effect of the large buoyancy and wake flow, the bubble necking rapidly shrinks and the bubble shape

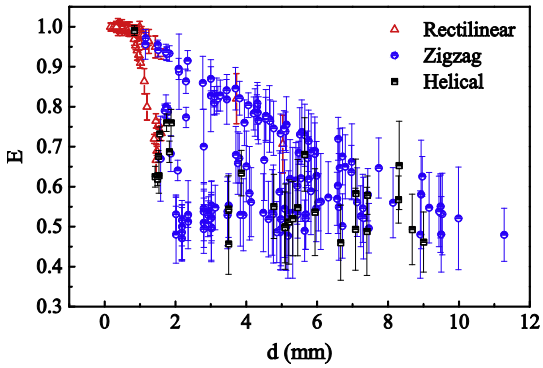

Fig. 13. Bubble aspect ratio E vs. bubble diameter d in water.

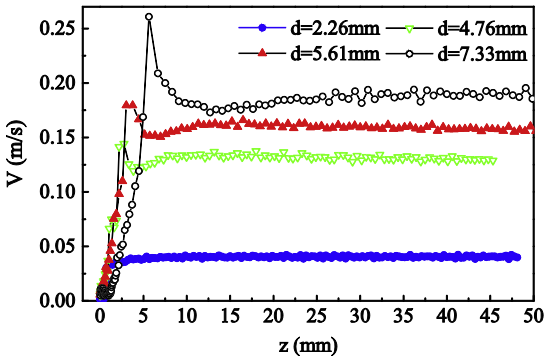

Fig. 15. Bubble instantaneous velocity vs. distance above the nozzle surface.

deforms to be flat, resulting in a large displacement of the center of gravity of the projection bubble, which lead to the appearance of the peak velocity. After that, the bubble is being compressed continually in the vertical direction all the time, and finally the bubble shape tends to be spherical cap and keeps stable along the path. However, in Fig. 17, the bubble shape, which is dominated by the surface tension and viscous force because of the small bubble diameter, remains spherical in the formation process, and the bubble necking connecting to the nozzle is fairly short. Hence, when the bubble detaches from the nozzle, the displacement of the center of gravity of the projection of the bubble barycenter caused by contraction of the bubble necking is very small and the peak velocity would not appear in this case.

3.3. Bubble shape and aspect ratio

3.3.1. Bubble shape

Original images of bubbles with different diameters generated under various nozzle diameters in water are shown in Figs. 18 and 19. In addition, bubble aspect ratio and terminal velocity as a function of bubble diameter is plotted in Fig. 20. As shown in Figs. 18 and 19, with the increase of bubble diameter, the bubble shape deforms from spherical to ellipsoidal, then to oblate ellipsoidal, finally to an irregular shape similar to cap with the surface wobbling strongly. However, it is the obvious that shapes of the bubbles, aspect ratio and bubble terminal velocity vary greatly in the condition that bubble diameters are nearly the same compared bubbles in Figs. 18 and 19. This indicates that bubble shapes, aspect ratio and terminal velocity in water are dramatically influenced by the nozzle diameters, i.e. the bubble dynamics is sensitive to the disturbance of detachment process. When the nozzle diameter is smaller than the bubble, the bubble will bears larger disturbance as it detaches from the nozzle, consequently, the deformation is larger and the bubble surface has an larger oscillation, leading to a lower aspect ratio and a greater terminal velocity and vice versa. Conversely, due to the small disturbance, the bubble deformation and surface oscillation is quite small and the bubble shape is easy to maintain stable.

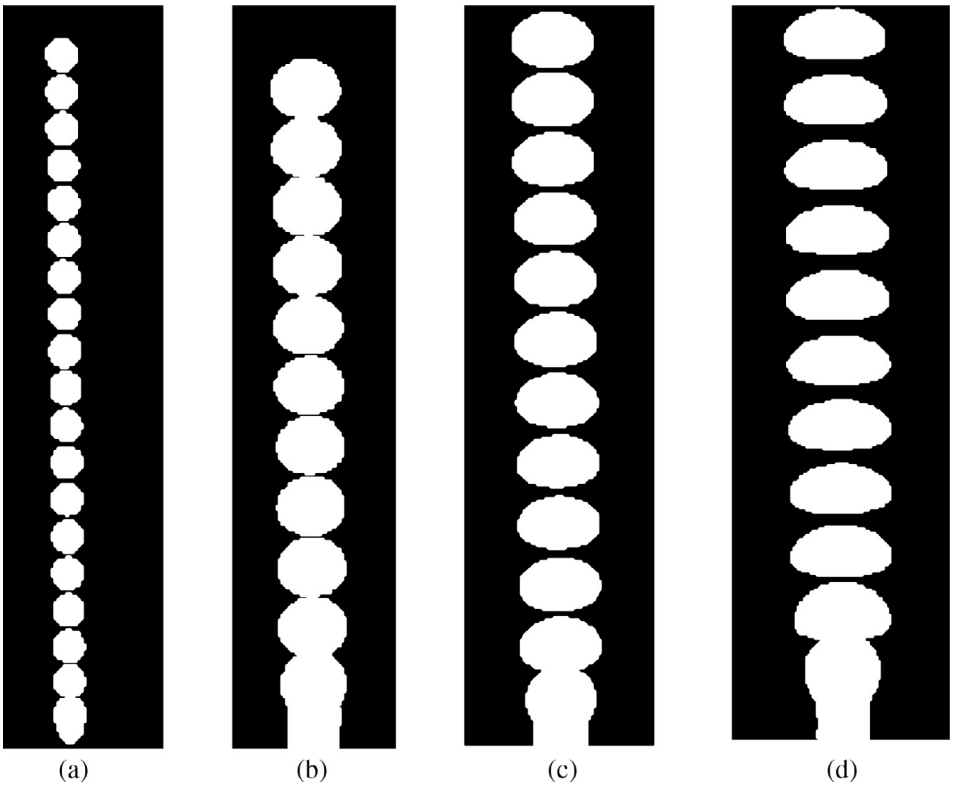

Fig. 14. The trajectory of bubbles with different diameters (a) d = 2.26 mm; (b) d = 4.76 mm; (c) d = 5.61 mm; (d) d = 7.33 mm.

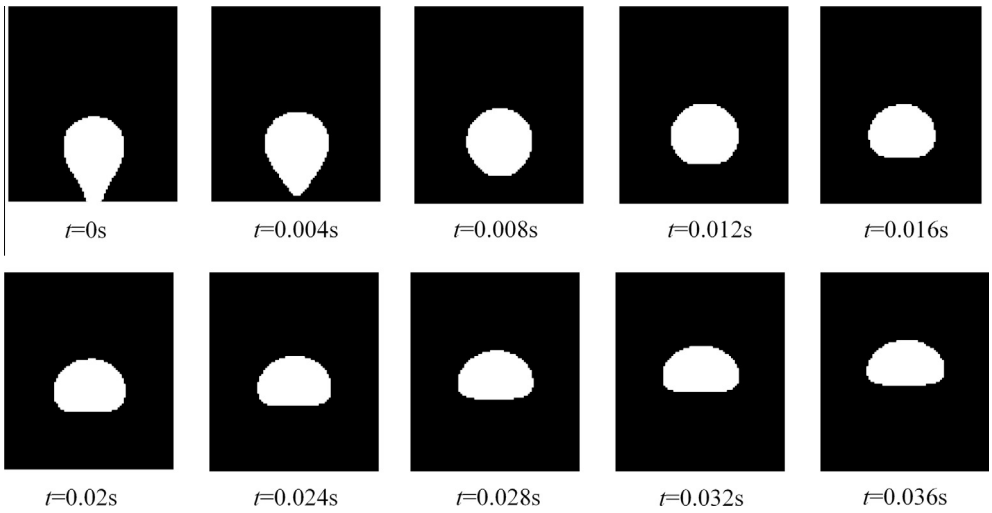

Fig. 16. Consecutive bubble images at different time of the bubble of d = 7.33 mm.

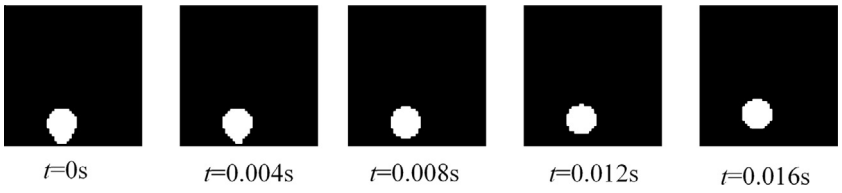

Fig. 17. Consecutive bubble images at different time of the bubble of d = 2.26 mm.

Fig. 21 shows the pictures of bubble shape changes in glycerol water solution S4 under different nozzle diameters. The bubble shape deforms from spherical to ellipsoidal, then to spherical cap, and the bubble shape keeps stability without surface oscillation with the increase of bubble diameter. Compared Fig. 21 with Figs. 18 and 19, owing to the effect of great viscous force, the bubble shape in glycerin water solution is more stable than that in the water, and without surface oscillating. Because of the viscosity of S1, S2, S3 is greater than that in S4, we found that all of the bubbles shape in S1, S2 and S3 is more stable and without surface wobbling.

3.3.2. Aspect ratio

A lot of attempts have been made to correlate the aspect ratio, E, as a function of dimensionless parameter, such as Eo [23,24], We [23,25–28] and Ta [29–31].

In contaminated liquids, Wellek et al. [23] developed a correlation for non-oscillating drops, as indicated in Eq. (2), and later Fan and Tsuchiya [31] found it suitable to oscillating bubbles in low-viscosity liquids.

$$E = \frac{1}{1 + 0.163Eo^{0.757}} \tag{2}$$

Okawa et al. [24] modified the coefficient of the above correlation and proposed the following correlation, in order to fit the lower boundary of their experimental data.

$$E = \frac{1}{1 + 1.97Eo^{1.3}} \tag{3}$$

Figs. 22 and 23 show the plot of E as a function of Eo, along with Eqs. (2) and (3) in water and glycerol aqueous solution, respectively.

In water, the Wellek correlation, Eq. (2) correlates the aspect ratio fairly well for $Eo < 0.09$. The data begins to scatter for $Eo > 0.09$ and approaches the upper bound of data, which indicates that the Wellek correlation fails to group the data well. The Okawa correlation, Eq. (3), correlates the aspect ratio fairly well for $Eo < 0.03$ and approaches the lower bound of data globally. The results show good agreement with the data by Celata et al. [47,48]. In glycerin aqueous solution, the data are scattered severely, in addition, both the Wellek and Okawa correlation underestimate the aspect ratio. The Eo number represents the ratio of gravity and surface tension, without relating to influence of the inertia force, hence, when the bubble diameter is large enough and the bubble velocity increases to a certain value, the effect of inertial force would play the leading role on the bubble shape and must be considered. This is already illustrated by Tomiyama et al. [11] and Celata et al. [47,48], therefore Eo is not the most appropriate parameter to group bubble shape data throughout the observed range.

By adopting the Weber number, We, Moore [27] derived the following expression using low order theory, which valid for $E > 0.5$,

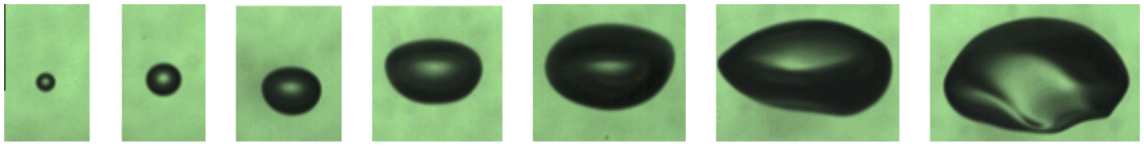

Fig. 18. Bubble shape in water (a) Do = 9.9 mm, d = 0.83 mm; (b) Do = 9.9 mm, d = 1.51 mm; (c) Do = 9.9 mm, d = 3.10 mm; (d) Do = 9.9 mm, d = 4.67 mm; (e) Do = 9.9 mm, d = 5.93 mm; (f) Do = 9.9 mm, d = 7.42 mm; (f) Do = 9.9 mm, d = 8.93 mm.

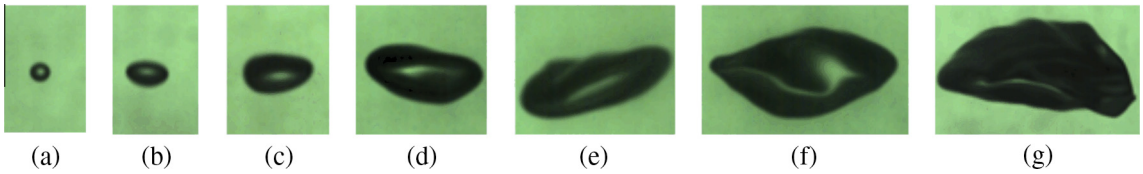

Fig. 19. Bubble shape in water (a) *Do* = 0.6 mm, *d* = 0.83 mm; (b) *Do* = 0.6 mm, *d* = 1.58 mm; (c) *Do* = 1.0 mm, *d* = 3.02 mm; (d) *Do* = 1.0 mm, *d* = 4.73 mm; (e) *Do* = 1.0 mm, *d* = 5.93 mm; (f) *Do* = 4.3 mm, *d* = 7.46 mm; (g) *Do* = 4.3 mm, *d* = 9.00 mm.

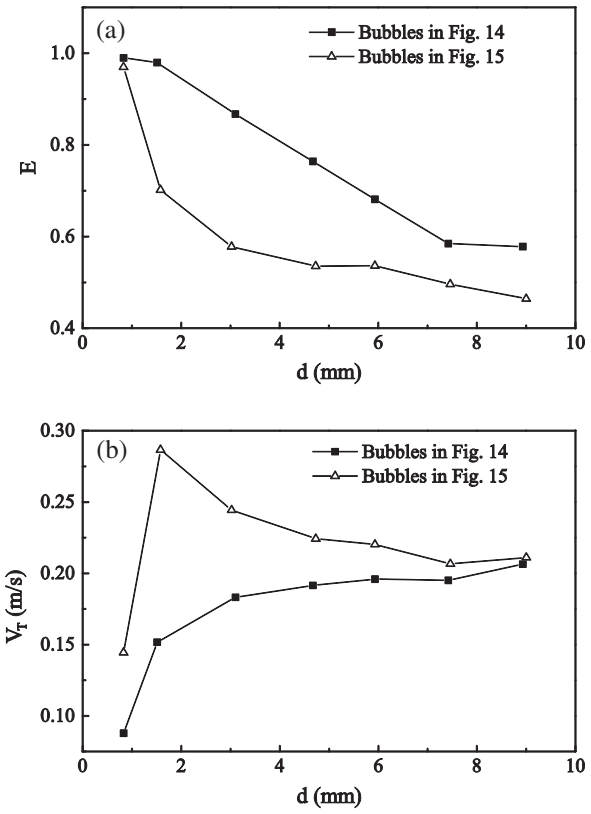

Fig. 20. Bubble aspect ratio and terminal velocity vs. bubble diameter in water.

assuming that the flow around the bubble surface is essentially nonviscous.

$$We = 4E^{1/3}\frac{1+E^2-2E^3\left[\cos^{-1}E - E\sqrt{1-E^2}\right]^2}{\left(1-E^2\right)^3} \tag{4}$$

Eq. (5) can be obtained by expanding Eq. (4) in Taylor series and truncating to the first term [25].

$$E = \frac{1}{1+9We/64} \tag{5}$$

While Taylor and Acrivos [26] proposed another model by expanding Eq. (4) in a series only considered the first term, and the result is shown in Eq. (6).

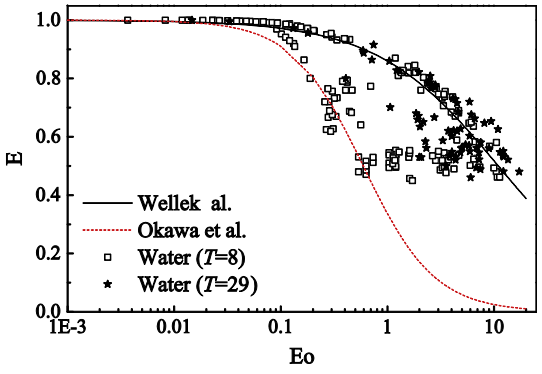

Fig. 22. Bubble aspect ratio vs. *Eo* number in water.

$$E = \frac{1}{1+5We/32} \tag{6}$$

Wellek et al. [23] proposed the following correlation for non-oscillating liquid drops in fairly contaminated liquids.

$$E = \frac{1}{1+0.091We^{0.95}} \tag{7}$$

Kelbaliyev and Ceylan [28] proposed the following correlation based on Weber and Reynolds number by using the experimental data from Raymond and Rosant [10].

$$E = \frac{1-\lambda_v We}{1+\frac{\lambda_v}{2}We} \tag{8}$$

where

$$\lambda_v = \frac{1}{12}\left(1-\frac{3}{25}\frac{We}{Re}\right)$$

Figs. 24 and 25 show the plot of *E* as a function of *We*, along with Eqs. (4)–(8) in water and glycerol aqueous solution, respectively. From Fig. 24, we can see that the aspect ratio data lies on the same curve and decreases almost linearly with the *We* up to 0.6, then tends to scatter with the *We*, but the scatter degree is much smaller than that in Fig. 22. Therefore, in the water with low viscosity, the *We* is more suitable to correlate the bubble shape than *Eo*. It is also indicated that the deformation of the bubble is mainly dominated by the surface tension and inertia force in water. In addition, when *We* is small, all of the correlations can perfectly predict the trend of aspect ratio. But for *We* > 0.6, the Wellek

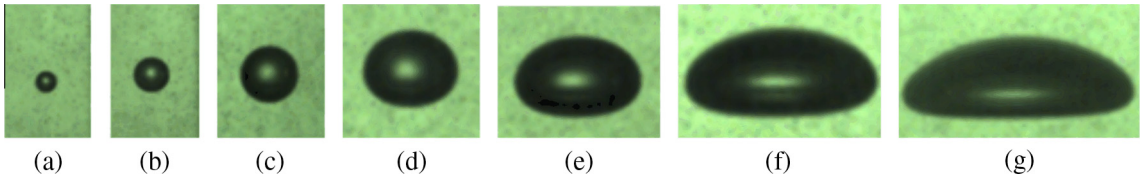

Fig. 21. Bubble shape in glycerol aqueous solution of S4 (a) *Do* = 0.6 mm, *d* = 0.86 mm; (b) *Do* = 0.6 mm, *d* = 1.51 mm; (c) *Do* = 1.0 mm, *d* = 2.88 mm; (d) *Do* = 1.0 mm, *d* = 4.76 mm; (e) *Do* = 1.0 mm, *d* = 6.03 mm; (f) *Do* = 4.3 mm, *d* = 7.52 mm; (g) *Do* = 4.3 mm, *d* = 9.61 mm.

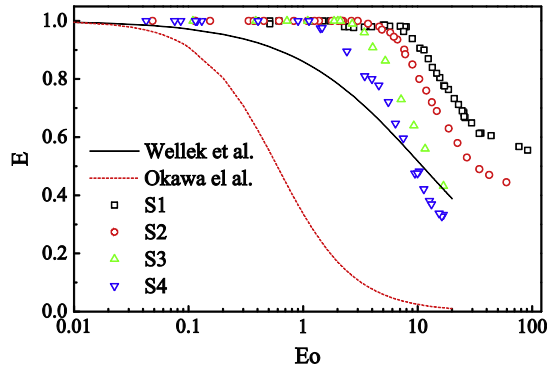

Fig. 23. Bubble aspect ratio vs. *Eo* number in glycerol aqueous solution.

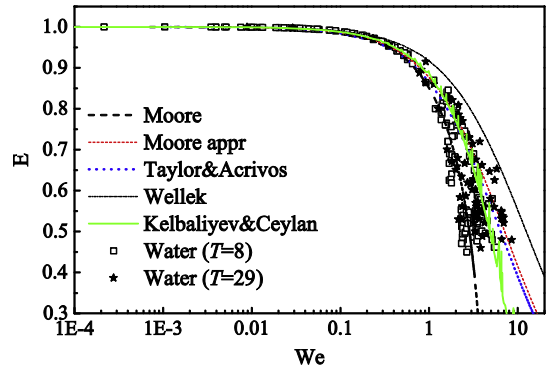

Fig. 24. Bubble aspect ratio vs. *We* number in water.

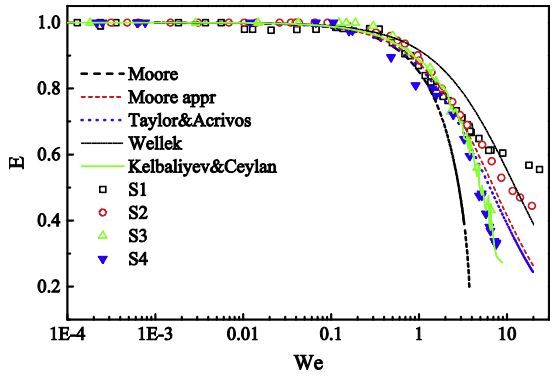

Fig. 25. Bubble aspect ratio vs. *We* number in glycerol aqueous solution.

correlation overestimates all the experimental data, and Moore correlation is close to the lower boundary of the experimental data, while the Taylor and Acrivos, Moore appr and Kelbaliyev can predict the aspect ratio well. Globally, the best prediction of the aspect ratio as a function of *We* is given by the Kelbaliyev and Ceylan correlation, Eq. (8).

In glycerol aqueous solution, as shown in Fig. 25, for $We < 0.2$, the aspect ratio remains 1, and the bubble keeps spherical. For $We > 0.2$, the aspect ratio decreases with *We*. While with the increase of *We* continually, the aspect ratio occurs to scatter. Especially for $We > 6$, the scattered trend of aspect ratio with *We* is very obvious in the highest viscosity fluid S1. When *We* is small, all of the correlation can perfectly predict the aspect ratio, but when *We* increases to large enough, the Wellek correlation overestimates the experimental data in most cases, while the Moore correlation generally underestimates the experimental data. As a whole, the correlations of Taylor and Acrivos, Moore appr and Kelbaliyev can predict the aspect ratio to some extent. It is known that the *We* cannot character the effect of the liquid viscosity on bubble shape, therefore, it is impossible to give a good prediction of bubble aspect ratio only using *We* for high viscosity fluid.

Tadaki and Maeda [29] introduced an original new dimensionless number, named Tadaki number, *Ta*, by experimental studies in various liquids and proposed the following correlation for the correlation of the aspect ratio.

$$E^{1/3} = \begin{cases} 1 & Ta < 2 \\ 1.14Ta^{-0.176} & 2 < Ta < 6 \\ 1.36Ta^{-0.28} & 6 < Ta < 16.5 \\ 0.62 & 16.5 < Ta \end{cases} \tag{9}$$

Later, Vakhrushev and Efremov [30] modified the above correlation for the calculation of the aspect ratio.

$$E = \begin{cases} 1 & Ta < Ta_1 \\ \{c_1 + c_2 \tanh[c_3(c_4 - \log_{10}Ta)]\}^2 & Ta_1 < Ta < Ta_2 \\ c_5 & Ta_2 < Ta \end{cases} \tag{10}$$

Fan and Tsuchiya [31] developed the above correlation and gave all the coefficients for a 2D pure fluid, i.e.

$$E = \begin{cases} 1 & Ta < 0.3 \\ \{0.77 + 0.24\tanh[1.9(0.4 - \log_{10}Ta)]\}^2 & 0.3 < Ta < 20 \\ 0.3 & 20 < Ta \end{cases} \tag{11}$$

The aspect ratio in the water and glycerol aqueous solution is plotted vs. the Tadaki number in Figs. 26 and 27, respectively, along with Eqs. (9) and (11). The Tadaki number is worse than

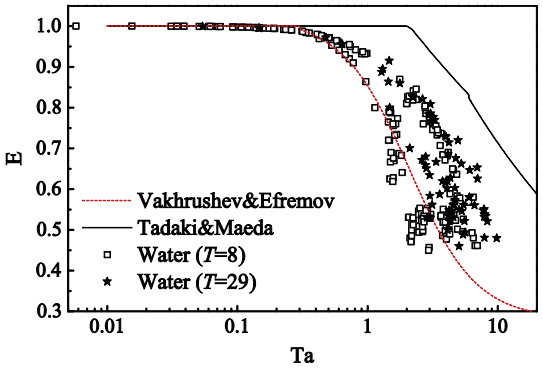

Fig. 26. Bubble aspect ratio vs. *Ta* number in water.

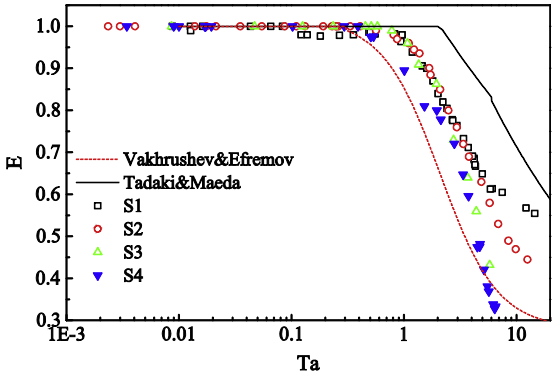

Fig. 27. Bubble aspect ratio vs. *Ta* number in glycerol aqueous solution.

Table 2
Undetermined coefficient, standard deviation, residual sum of squares and correlation coefficient.

Liquid phase	Dimensionless parameter	*a*	*b*	*c*	*StD*	*SSE*	*r*
Water $n = 256$	*Eo*	0.6068	0.8122	0.1958	0.1153	3.4027	0.7786
	We	0.9722	0.2752	0.816	0.0787	1.3618	0.9082
	Re	0.8678	0.0297	0.4759	0.1077	2.9724	0.810
	Ta	0.9246	0.2948	0.6792	0.0960	2.361	0.8526
Glycerol aqueous solution $n = 123$	*Eo*	0.9476	0.0645	0.7343	0.1239	1.8891	0.7846
	We	0.9862	0.1894	0.8066	0.0615	0.4649	0.9518
	Re	0.98220	0.0977	0.7725	0.08279	0.8431	0.910
	Ta	0.9827	0.1038	1.1949	0.0664	0.5417	0.9437

Table 3
Undetermined coefficient, standard deviation, residual sum of squares and correlation coefficient.

Liquid phase	Dimensionless parameter	*a*	*b*	*c*	*e*	*StD*	*SSE*	*r*
Water $n = 256$	*We* and *Eo*	0.9948	0.1535	1.7047	−0.4052	0.0613	0.9627	0.9427
Glycerin aqueous solution $n = 123$	*We* and *Re*	0.9914	0.1147	0.5678	0.3841	0.0398	0.1951	0.9799

the Weber number, better than the Eötvös number in correlating the aspect ratio. The Tadaki and Maeda correlation is not suitable to predict the present data, showing that overestimates the experimental data in both water and glycerol aqueous solution. Better predictions are provided by Vakhrushev and Efremov correlation for water data, which is close to the lower boundary, nevertheless, it generally underestimates the data in glycerol aqueous solution. Tadaki number weakens the effect of liquid viscosity on bubble shape. Consequently, it is not suitable as the characteristic parameter to describe the bubble deformation in the fluid with high viscosity.

3.3.3. Empirical correlation of aspect ratio

Figs. 22–27 show that the aspect ratio generally decreases with the increase of dimensionless numbers (*Eo*, *We* and *Ta*). Therefore, the following correlation can be used to predict the bubble aspect ratio:

$$E = \frac{1}{a + b \cdot IL^c} \tag{12}$$

The *Eo*, *We*, *Re* or *Ta* number is respectively used as the dimensionless number, *IL*, and substituted into Eq. (12). Then the undetermined coefficients (*a*, *b*, *c*), standard deviation, residual sum of squares, correlation coefficient are obtained by applying the least-square fitting with the experimental data, and the results are shown in Table 2.

Table 2 shows that, in water and glycerin aqueous solution, the best prediction is provided by using *We*, with the smallest *StD*, *SSE* and largest *r*. Therefore, as analyzed above, the *We* is the best parameter to correlate the aspect ratio globally. However, the above analysis also showed that, with the increase of both bubble diameter and fluid viscosity, the gravitational force and viscous force are playing a more and more important role on the bubble shape, which cannot be negative. In this instance, the effects of gravity and viscous force should be taken consideration, that is, the prediction model in Eqs. (13) and (14) will be modified by overall considering the effects of We, *Eo* or *We* and *Re* number in water and glycerin aqueous solution, respectively, and the results are shown in Table 3.

$$E = \frac{1}{a + b \cdot We^c \cdot Eo^e} \tag{13}$$

$$E = \frac{1}{a + b \cdot We^c \cdot Re^e} \tag{14}$$

The corresponding parameters in Table 3 are all better than those in Table 2, which indicate that the combination of *We* and *Eo*, or *We* and *Re* as the dimensionless parameter is more suitable than that only using *Eo*, *We*, *Re* or *Ta* in correlating the aspect ratio with experimental data in present fluids.

To sum up, the best dimensionless parameter to correlate bubble shape in the present experiment for water data would therefore be the Weber number, while *Eo* and *Ta* are not suitable for the prediction of the bubble aspect ratio, evidencing that the bubble shape is mainly controlled by inertial force and surface tension, and the effect of viscous force can be neglect. But when the bubble diameter is large enough, the effect of gravity should be taken into consideration in predicting the bubble shape. However, in glycerin aqueous solution with high viscosity, when the bubble diameter is large enough, due to that the bubble shape is affected by viscosity dramatically. Hence, it is not suitable to predict bubble deformation only using one dimensionless numbers, which should be required overall considering the effects of *We*, *Eo* or *We*, *Re* number.

4. Conclusions

The single bubble dynamics rising in water and glycerin water solution were conducted in this paper based on high-speed photography and image processing technology. Based on the experimental results, several conclusions can be drawn as follows:

(1) The bubble terminal velocity increases while aspect ratio decreases almost linearly with bubble diameter in the viscous force dominant regime and bubble trajectory all keeps rectilinear. Both terminal velocity and aspect ratio begin to widely scatter while bubble trajectory is likely to remain rectilinear or switch to be zigzag or helical with diameter increasing in the surface tension force dominant regime. As a whole, the terminal velocity seems to be higher while aspect ratio to be lower for bubbles with helical trajectories than those bubbles with zigzag trajectories in this regime. The level of scatter tends to be quite weak and terminal velocity increases while aspect ratio decrease gradually in the inertial force dominant regime and the bubble motion could be either zigzag or helical, without rectilinear motions occurring.

(2) In the water with low viscosity, the bubble aspect ratio, on the whole, can be correlated with *We*, while *Eo* and *Ta* are not suitable for the prediction of the bubble aspect ratio. The bubble shape is mainly dominated by the inertial force

and surface tension in water, and the effect of viscous force is small. When the bubble diameter is quite large, it is necessary to consider the effect of gravity on the bubble shape.

(3) In glycerin water solution with high viscosity, any single dimensionless number *Eo*, *We* or *Ta* is not suitable for the prediction of the bubble deformation. It has to consider the impact of *We* and *Re* on the bubble shape.

(4) The best prediction models of the aspect ratio *E* are respectively shown in Eq. (13) and (14) by using the *We*, *Eo* and *We*, *Re* for water and glycerin water solution.

Acknowledgments

This work was financially supported by the Postdoctoral Science Foundation of Central South University (Project No. 111033), Hunan Provincial Innovation Foundation for Postgraduate (Project No. CX2014B063), and the National High-Tech Research and Development Program of China (Project No. 2011AA061003).

References

[1] J.R. Grace, T. Wairegi, T.H. Nguyen, Shapes and velocities of single drops and bubbles moving freely through immiscible liquids, Trans. IChemE. 54 (3) (1976) 167–173.
[2] R. Clift, J.R. Grace, M.E. Weber, Bubbles, Drops and Particles, Academic Press, New York, 1978.
[3] D. Bhaga, M.E. Weber, Bubbles in viscous liquids: shapes, wakes and velocities, J. Fluid Mech. 105 (1) (1981) 61–85.
[4] L. Rayleigh, On the pressure developed in a liquid during the collapse of a spherical cavity, Philos. Mag. 34 (1917) 94–98.
[5] M.S. Plesset, R.B. Chapman, Collapse of an initially spherical vapour cavity in the neighbourhood of a solid boundary, J. Fluid Mech. 47 (1971) 283–290.
[6] M.S. Plesset, A. Prosperetti, Bubble dynamics and cavitation, Annu. Rev. Fluid Mech. 9 (1) (1977) 145–185.
[7] A. Prosperetti, A. Lezzi, Bubble dynamics in a compressible liquid. Part 1. First-order theory, J. Fluid Mech. 168 (1986) 457–478.
[8] A. Lezzi, A. Prosperetti, Bubble dynamics in a compressible liquid. Part 2. Second-order theory, J. Fluid Mech. 185 (1987) 289–321.
[9] T. Maxworthy, C. Gnann, M. Kürten, et al., Experiments on the rise of air bubbles in clean viscous liquids, J. Fluid Mech. 321 (1996) 421–441.
[10] F. Raymond, J.M. Rosant, A numerical and experimental study of the terminal velocity and shape of bubbles in viscous liquids, Chem. Eng. Sci. 55 (5) (2000) 943–955.
[11] A. Tomiyama, G.P. Celata, S. Hosokawa, et al., Terminal velocity of single bubbles in surface tension force dominant regime, Int. J. Multiphase Flow 28 (9) (2002) 1497–1519.
[12] M. Maldonado, J.J. Quinn, C.O. Gomez, et al., An experimental study examining the relationship between bubble shape and rise velocity, Chem. Eng. Sci. 98 (2013) 7–11.
[13] D. Mikaelian, A. Larcy, S. Dehaeck, et al., A new experimental method to analyze the dynamics and the morphology of bubbles in liquids: application to single ellipsoidal bubbles, Chem. Eng. Sci. 100 (2013) 529–538.
[14] Y. Nagami, T. Saito, An experimental study of the modulation of the bubble motion by gas–liquid-phase interaction in oscillating-grid decaying turbulence, Flow Turbul. Combust. 92 (1–2) (2014) 147–174.
[15] M. van Sint Annaland, N.G. Deen, J.A.M. Kuipers, Numerical simulation of gas bubbles behaviour using a three-dimensional volume of fluid method, Chem. Eng. Sci. 60 (11) (2005) 2999–3011.
[16] T. Bonometti, J. Magnaudet, An interface-capturing method for incompressible two-phase flows. Validation and application to bubble dynamics, Int. J. Multiphase Flow 33 (2) (2007) 109–133.
[17] J. Hua, J.F. Stene, P. Lin, Numerical simulation of 3D bubbles rising in viscous liquids using a front tracking method, J. Comput. Phys. 227 (6) (2008) 3358–3382.
[18] Z. Yu, H. Yang, L.S. Fan, Numerical simulation of bubble interactions using an adaptive lattice Boltzmann method, Chem. Eng. Sci. 66 (14) (2011) 3441–3451.
[19] M.R. Pivello, M.M. Villar, R. Serfaty, et al., A fully adaptive front tracking method for the simulation of two phase flows, Int. J. Multiphase Flow 58 (2014) 72–82.
[20] Q. Zeng, J. Cai, Three-dimension simulation of bubble behavior under nonlinear oscillation, Ann. Nucl. Energy 63 (2014) 680–690.
[21] A. Gupta, R. Kumar, Lattice Boltzmann simulation to study multiple bubble dynamics, Int. J. Heat Mass Transfer 51 (21) (2008) 5192–5203.
[22] S. Anwar, Lattice Boltzmann modeling of buoyant rise of single and multiple bubbles, Comput. Fluids 88 (2013) 430–439.
[23] R.M. Wellek, A.K. Agrawal, A.H.P. Skelland, Shape of liquid drops moving in liquid media, AIChE J. 12 (5) (1966) 854–862.
[24] T. Okawa, T. Tanaka, I. Kataoka, et al., Temperature effect on single bubble rise characteristics in stagnant distilled water, Int. J. Heat Mass Transfer 46 (5) (2003) 903–913.
[25] D.W. Moore, The rise of a gas bubble in a viscous liquid, J. Fluid Mech. 6 (1) (1959) 113–130.
[26] T.D. Taylor, A. Acrivos, On the deformation and drag of a falling viscous drop at low Reynolds number, J. Fluid Mech. 18 (3) (1964) 466–476.
[27] D.W. Moore, The velocity of rise of distorted gas bubbles in a liquid of small viscosity, J. Fluid Mech. 23 (4) (1965) 749–766.
[28] G. Kelbaliyev, K. Ceylan, Development of new empirical equations for estimation of drag coefficient, shape deformation, and rising velocity of gas bubbles or liquid drops, Chem. Eng. Commun. 194 (12) (2007) 1623–1637.
[29] T. Tadaki, S. Maeda, On the shape and velocity of single air bubbles rising in various liquids, Kagaku Kogaku 25 (1961) 254–264.
[30] I.A. Vakhrushev, G.I. Efremov, Chem. Technol. Fuel Oils (USSR) 5 (6) (1970) 376–379 (cited by Clift et al., 1978).
[31] L.S. Fan, K. Tsuchiya, Bubble Wake Dynamics in Liquids and Liquid–Solid Suspensions, Butterworth-Heinemann, Oxford, 1990.
[32] M. Wu, M. Gharib, Experimental studies on the shape and path of small air bubbles rising in clean water, Phys. Fluids 14 (7) (2002) 49–52.
[33] A.W.G. de Vries, A. Biesheuvel, L. Van Wijngaarden, Notes on the path and wake of a gas bubble rising in pure water, Int. J. Multiphase Flow 28 (11) (2002) 1823–1835.
[34] C. Veldhuis, A. Biesheuvel, L. Van Wijngaarden, Shape oscillations on bubbles rising in clean and in tap water, Phys. Fluids 20 (4) (2008) 040705.
[35] R. Zenit, J. Magnaudet, Path instability of rising spheroidal air bubbles: a shape-controlled process, Phys. Fluids 20 (6) (2008) 061702.
[36] P.G. Saffman, On the rise of small air bubbles in water, J. Fluid Mech. 1 (03) (1956) 249–275.
[37] T.B. Benjamin, Hamiltonian theory for motions of bubbles in an infinite liquid, J. Fluid Mech. 181 (1987) 349–379.
[38] C. Brücker, Structure and dynamics of the wake of bubbles and its relevance for bubble interaction, Phys. Fluids 11 (1999) 1781.
[39] K. Ellingsen, F. Risso, On the rise of an ellipsoidal bubble in water: oscillatory paths and liquid-induced velocity, J. Fluid Mech. 440 (1) (2001) 235–268.
[40] G.G. Stokes, J.W.S.B. Rayleigh, Mathematical and Physical Papers, Cambridge University Press, London, 1880.
[41] R.M. Davies, G. Taylor, The mechanics of large bubbles rising through extended liquids and through liquids in tubes, Proc. R. Soc. Lond., Ser. A 200 (1062) (1950) 375–390.
[42] W.L. Haberman, R.K. Morton, An experimental study of bubbles moving in liquids, Trans. Am. Soc. Civil Eng. 121 (1) (1956) 227–250.
[43] H.D. Mendelson, The prediction of bubble terminal velocities from wave theory, AIChE J. 13 (2) (1967) 250–253.
[44] D. Rodrigue, D. De Kee, C.F. Chan Man Fong, An experimental study of the effect of surfactants on the free rise velocity of gas bubbles, J. Nonnewton. Fluid Mech. 66 (2) (1996) 213–232.
[45] N.M. Aybers, A. Tapucu, The motion of gas bubbles rising through stagnant liquid, Wärme Stoffübertragung 2 (2) (1969) 118–128.
[46] N.M. Aybers, A. Tapucu, Studies on the drag and shape of gas bubbles rising through a stagnant liquid, Wärme Stoffübertragung 2 (3) (1969) 171–177.
[47] G.P. Celata, M. Cumo, F. D'Annibale, et al., Effect of gas injection mode and purity of liquid on bubble rising in two-component systems, Exp. Therm. Fluid Sci. 31 (1) (2006) 37–53.
[48] G.P. Celata, F. D'Annibale, P. Di Marco, et al., Measurements of rising velocity of a small bubble in a stagnant fluid in one-and two-component systems, Exp. Therm. Fluid Sci. 31 (6) (2007) 609–623.